LANGMUIR Article
Cite This: Langmuir 2019, 35, 4197−4204
pubs.acs.org/Langmuir

Apparent Contact Angles on Lubricant-Impregnated Surfaces/SLIPS: From Superhydrophobicity to Electrowetting

Glen McHale,* Bethany V. Orme, Gary G. Wells, and Rodrigo Ledesma-Aguilar

Smart Materials & Surfaces Laboratory, Faculty of Engineering & Environment, Northumbria University, Newcastle upon Tyne NE1 8ST, U.K.

ABSTRACT: A fundamental limitation of liquids on many surfaces is their contact line pinning. This limitation can be overcome by infusing a nonvolatile and immiscible liquid or lubricant into the texture or roughness created in or applied onto the solid substrate so that the liquid of interest no longer directly contacts the underlying surface. Such slippery liquid-infused porous surfaces (SLIPS), also known as lubricant-impregnated surfaces, completely remove contact line pinning and contact angle hysteresis. However, although a sessile droplet may rest on such a surface, its contact angle can be only an apparent contact angle because its contact is now with a second liquid and not a solid. Close to the solid, the droplet has a wetting ridge with a force balance of the liquid−liquid and liquid−vapor interfacial tensions described by Neumann's triangle rather than Young's law. Here, we show how, provided the lubricant coating is thin and the wetting ridge is small, a surface free energy approach can be used to obtain an apparent contact angle equation analogous to Young's law using interfacial tensions for the lubricant−vapor and liquid−lubricant and an effective interfacial tension for the combined liquid−lubricant−vapor interfaces. This effective interfacial tension is the sum of the liquid−lubricant and the lubricant−vapor interfacial tensions or the liquid−vapor interfacial tension for a positive and negative spreading power of the lubricant on the liquid, respectively. Using this approach, we then show how Cassie−Baxter, Wenzel, hemiwicking, and other equations for rough, textured or complex geometry surfaces and for electrowetting and dielectrowetting can be used with the Young's law contact angle replaced by the apparent contact angle from the equivalent smooth lubricant-impregnated surface. The resulting equations are consistent with the literature data. These results enable equilibrium contact angle theory for sessile droplets on surfaces to be used widely for surfaces that retain a thin and conformal SLIPS coating.

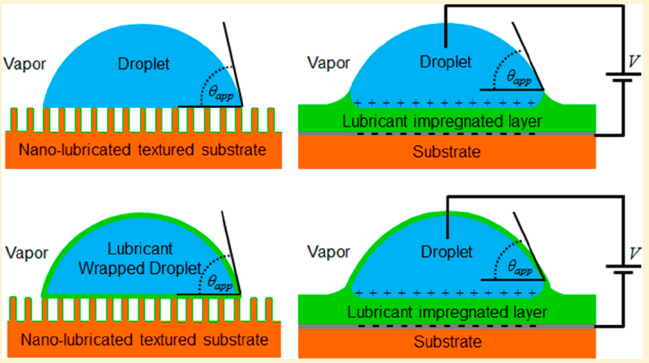

1. INTRODUCTION

A fundamental underpinning concept when dealing with droplets on surfaces is the Young's law contact angle (θ_Y) defined by

$$\cos\theta_Y = \frac{(\gamma_{SV} - \gamma_{SL})}{\gamma_{LV}} \quad (1)$$

where the γ_{IJ} represents the interfacial tensions for the solid−vapor, solid−liquid, and liquid−vapor interfaces.[1] However, in experiments, the measured angles are the static contact angle (θ_S), advancing contact angle (θ_A), receding contact angle (θ_R), and dynamic contact angle (θ_D), none of which match the contact angle given by Young's law.[2−4] This reflects the contact line pinning and contact angle hysteresis, $\Delta\theta_{CAH} = (\theta_A - \theta_R)$, arising from the intrinsically heterogeneous nature of substrates due to small-scale roughness and surface chemistry. In a typical sessile droplet measurement, the observed static contact angle has a value intermediate between the advancing and receding contact angles, whose range defines the contact angle hysteresis. The existence of contact line pinning has multiple consequences, from the need to provide sufficient force to overcome the contact line pinning before droplet (or contact line) motion can occur in a microfluidic system to the formation of ring stains during the drying of droplets.[5,6]

Recently, the concept of slippery liquid-infused porous surfaces (SLIPS), or equivalently lubricant-impregnated surfaces, has been introduced to overcome contact line pinning.[7−9] On these surfaces, sessile-type droplets are observed and apparent contact angles can be defined despite the paradox that the droplet rests on a lubricant and never actually contacts the underlying solid surface.[10] Thus, contact line pinning causing contact angle hysteresis is removed, but so is the concept of a Young's law contact angle. Conceptually, the system becomes the limit of a liquid lens (droplet) on a shallow pool of (lubricant) liquid with the concept of the contact angle replaced by the balance among three interfacial tensions for the liquid−lubricant−liquid system in a Neumann triangle.[11,12] Moreover, if the spreading power for the lubricant liquid on the liquid of the droplet is positive, then the droplet

Received: December 13, 2018
Revised: February 9, 2019
Published: February 13, 2019

DOI: 10.1021/acs.langmuir.8b04136
Langmuir 2019, 35, 4197−4204

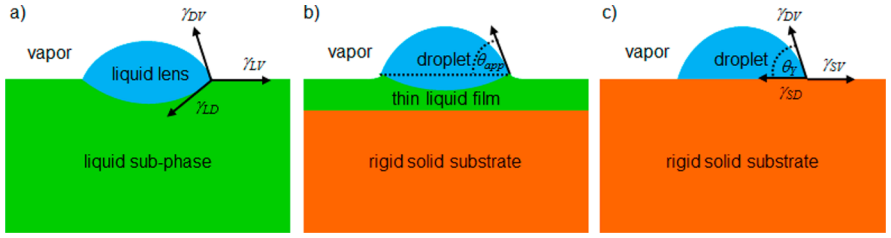

Figure 1. (a) Liquid lens on a deep liquid subphase with a Neumann triangle of forces, (b) a droplet on a thin liquid film on a rigid solid substrate, and (c) a droplet obeying Young's law on a rigid solid substrate.

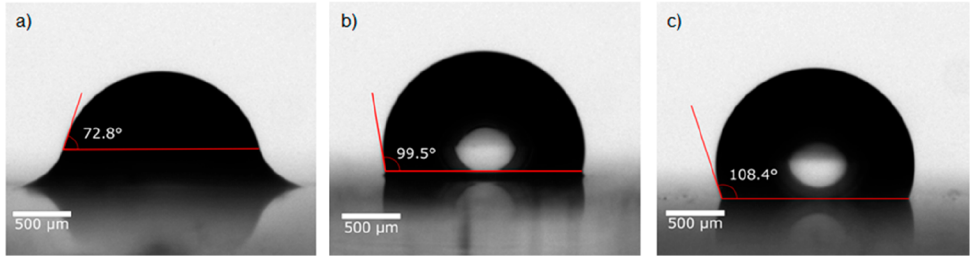

Figure 2. Experimental side-profile views of small droplets of water on SLIP surfaces with (a) a visible wetting ridge, (b) a small wetting ridge, and (c) no visibly obvious wetting ridge.

may be fully coated in a thin layer of the lubricant,[8] further complicating any interpretation arising from contact angle approaches.

From the perspective of droplets on soft substrates, Young's law and Neumann's triangle are the two extremes in the wetting behavior in the limits of an infinitely hard substrate (i.e., solid) and an infinitely soft (i.e., liquid) substrate.[13] It is possible to imagine a transition from a liquid lens on a liquid subphase to a sessile droplet on a solid surface as the liquid subphase becomes ever thinner and which in the extreme limit has vanishing thickness (Figure 1). Experimentally, lubricant coatings on a solid substrate can be created, which are extremely thin (typically <1 μm), so a question arises about how concepts arising from contact angle theory can be applied in this limit. In contact angle theory, the interfacial tensions can be regarded as either forces per unit length or surface free energies per unit area. The use of a surface free energy approach enables simple derivations of Young's law on a smooth surface, Wenzel and Cassie–Baxter equations on topographical rough and textured surfaces,[3,14] the Young–Lippmann electrowetting-on-dielectric contact angle,[15] and the effect on the contact angles of interface-localized dielectrophoresis (dielectrowetting).[16] Because SLIPS coatings have been used experimentally with topographically structured surfaces (e.g., SLIPS Wenzel[17] and SLIPS Cassie–Baxter[17,18] states) and with both electrowetting[19−22] and dielectrowetting,[21] it would be extremely useful if a similar simple approach could be applied to SLIP surfaces in the limit of thin film coatings.

In this work, we show how a surface free energy approach can be used to derive the apparent equilibrium contact angle for droplets on SLIP surfaces with thin conformal lubricant films. We show how this argument can be applied to topographically structured surfaces, such as those used in superhydrophobicity, roughness-induced wetting, and hemiwicking, to surfaces with complex geometry or shape, and to electrowetting and dielectrowetting. We also show that the results are consistent with literature data. Our work therefore provides a conceptual framework for apparent equilibrium contact angles for droplets and contact lines, which is widely applicable to surfaces with thin conformal SLIPS, lubricant-impregnated coatings, or lubricant coatings.

2. SLIP SURFACES

Lubricant-impregnated surfaces can be created using a wide variety of material techniques. These include using porous layers,[7] electrospinning,[23] membranes,[24] lithographically fabricated textures,[8,10] particle coatings,[25,26] sand-blasting and boehimite,[27] etching,[28] electrodeposition,[29] and roll-to-roll nanoimprint lithography[30] of surfaces. The principle is to increase the solid surface area through roughness/texture or other means and ensure it is either intrinsically hydrophobic or has a hydrophobic surface coating; if the droplet of interest is not water, then the surface chemistry is chosen to be repellent to that liquid. A lubricant is chosen to be nonvolatile, to completely and preferentially wet the solid and be locked into the surface structure by the balance of interfacial tensions, and to be immiscible to the liquid in the droplet. The hydrophobicity (or liquid repellence) of the solid surface ensures that the lubricant is not displaced by the water (liquid) in the droplet. Under these circumstances, a droplet rests entirely on the lubricant and never contacts the underlying solid (similar to Figure 1b). The motion of a droplet contact line then always occurs on the lubricant whether it is advancing or receding, and this leads to complete mobility of the contact line and, hence, the droplet. Smith et al. provide an overview of the possible states of droplets on lubricant-impregnated surfaces, including ones in which partial contact with the underlying solid occurs.[8] From one perspective, a surface suitable for impregnation, prior to lubricant being infused, can be considered to be a Wenzel (e.g., hemiwicking) or a Cassie–Baxter (e.g., superhydrophobic)-type surface interpreted in the most general sense.[14] The process of infusing a lubricant often uses withdrawal from a lubricant bath, which leaves a film of thickness determined by the withdrawal speed and lubricant properties that can be estimated using the Landau–Levich–Derjaguin (LLD) equation.[31] Such films can be ∼1−100 μm thick, and this can be reduced by applying shear stress (e.g., by rinsing with water or spinning) until a thin thermodynamically

DOI: 10.1021/acs.langmuir.8b04136
Langmuir 2019, 35, 4197−4204

stable film is obtained. One complication in the choice of a lubricant (referred to here as "oil" to avoid notational confusion with liquid for the droplet) is whether its interfacial tensions favor it spreading on the liquid−vapor interface of the droplet. Thus, if the interfacial energy for the combined droplet−oil and oil−vapor interfaces is less than the interfacial energy for the droplet−vapor interface, $\gamma_{DO} + \gamma_{OV} < \gamma_{DV}$, then a film of oil will coat (wrap) the droplet. This is simply a statement that a positive (or zero) spreading power for oil on the liquid droplet in the presence of vapor

$$S_{OD}^{V} = \gamma_{DV} - \gamma_{DO} - \gamma_{OV} \geq 0 \tag{2}$$

favors an oil-film-coated droplet. Conversely, lubricant oils where the spreading power is negative will not self-coat in a film of the lubricant.

Figure 2 shows three examples of small droplets of water, viewed in a side profile, on SLIP surfaces, and in each case, it is possible to define an apparent contact angle, θ_{app}, from the profile; for a discussion of its definition, see Guan et al.[10] The size of the droplets is much less than the capillary length of water, $\kappa^{-1} = (\gamma_{LV}/\rho g)^{1/2}$, where ρ is the density and $g = 9.81$ ms^{-2} is the acceleration due to gravity, so the majority of their profile conforms to spherical caps. In Figure 2a, there is an obvious distortion close to the surface caused by a wetting ridge, whereas in Figure 2b a wetting ridge exists but at a significantly smaller length scale due to the thinness of the lubricant. In Figure 2c, there is no visibly obvious wetting ridge. The SLIP surfaces in Figure 2 were created using a superhydrophobic nanoparticle coating (Glaco Mirror Coat, Nippon Shine) on glass, which gives a static contact angle of 160° with contact angle hysteresis <10°. The surface in Figure 2a had 20 cSt viscosity silicone oil infused by withdrawal from a bath at 2 mm s^{-1}. This gave an oil thickness of (21.1 ± 0.1) μm measured by reflectometry and consistent with the LLD equation. This surface has an apparent contact angle of θ_{app} = 72.8° and a sliding angle of (0.1 ± 0.2)°, but a thick layer of excess oil is evidenced by the visibly significant wetting ridge. Reducing the withdrawal speed to 0.1 mm s^{-1} gives the thinnest controllable layer of oil (with our equipment for fabricating these surfaces) of (3.1 ± 0.4) μm with an apparent contact angle of θ_{app} = 99.5° and a sliding angle of (0.5 ± 0.2)° and with a significantly reduced wetting ridge (Figure 2b). Removing all excess oil by rinsing decreases the oil thickness to (1.9 ± 0.2) μm and increases the apparent contact angle to θ_{app} = 108.4° with an increase in the sliding angle to (3.4 ± 0.2)°.

The wetting ridge (lubricant skirt) for a droplet on a SLIP surface is caused by the balance of interfacial tensions at the droplet liquid−lubricant−vapor "contact line" close to the solid surface and is described by Neumann's triangle. In this interpretation, there is an effective interfacial force, γ_{eff}, given by

$$\gamma_{eff} = \begin{cases} \gamma_{DV} & S_{OD}^{V} < 0 \\ \gamma_{DO} + \gamma_{OV} & S_{OD}^{V} \geq 0 \end{cases} \tag{3}$$

For a thin lubricating film and droplet with a vanishingly small wetting ridge, it can be shown that the apparent contact angle can be approximated as[32] (also see ref 33)

$$\cos\theta_{app} = \frac{(\gamma_{OV} - \gamma_{OD})}{\gamma_{eff}} \tag{4}$$

This can be interpreted as Young's law for the apparent contact angle using the horizontal component of a net force balance per unit length of the apparent contact line but using an effective interfacial tension for the droplet−vapor interface (Figure 3; also see refs 32 and 33). Equation 4 no longer has

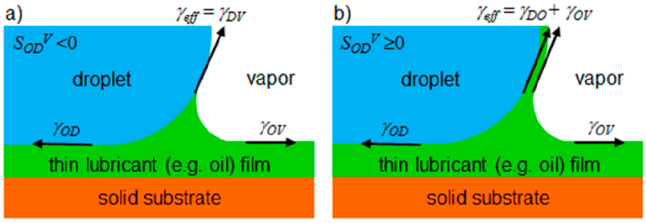

Figure 3. Schematic of a wetting ridge (a) without lubricant wrapping ($S_{OD}^{V} < 0$) and (b) with lubricant wrapping ($S_{OD}^{V} \geq 0$). Small-scale texture within which the lubricant is impregnated is omitted for clarity.

an explicit dependence on the interfacial tensions of the solid. For the surfaces in Figure 2, using γ_{DV} = 72.8 mN m^{-1}, γ_{OV} = 19.8 mN m^{-1} (measured), and γ_{OD} = 38 mN m^{-1} (data from Banpurkar et al.[34]) gives a positive spreading power of S_{OD}^{V} = 15.8 mN m^{-1}, and eq 4 predicts θ_{app} = 108.4°, which is the measured angle in Figure 2c; reducing γ_{OD} to 35 mN m^{-1} (data from Peters and Arabali[35]) reduces the prediction to θ_{app} = 106.1°. Literature data cited by Kreder et al.[33] in their Table 3 and Figure 1c, and from Rykaczewski et al.[36] suggests that eq 4 is a reasonable description of the observed apparent contact angles.

The work of Semprebon et al.[32] included an expression for the apparent contact angle of a droplet in contact with a wetting ridge that only partially wets the droplet. In the limit of small ridges relative to the size of the droplet, the apparent contact angle reaches a limiting upper-bound value. They showed that this can be understood in terms of the higher capillary pressure within smaller ridges, which effectively acts as line tension and leads to an increase in the apparent contact angle. Extrapolating this idea implies that eq 4 gives an upper bound to the value of the observed apparent contact angle for larger wetting ridges, consistent with the data in Figure 2.

3. SURFACE FREE ENERGY APPROACH

3.1. Apparent Equilibrium Contact Angle. The Young's law contact angle can be viewed as arising from a local equilibrium given by a local minimum in a surface free energy landscape close to the contact line and does not depend on the global shape of a droplet. Thus, the contact angle for a large gravitationally flattened droplet is, in principle, the same as for a small spherical cap-shaped droplet, although experimentally a difference may be observed as a result of the contact angle hysteresis. We therefore consider the droplet profile close to a solid surface having a thin lubricant-impregnated layer and consider small translational perturbations, ΔA, of the droplet edge along the lubricant interface, where we consider both $S_{OD}^{V} < 0$ and $S_{OD}^{V} \geq 0$ (Figure 4). In considering this translation, we assume the changes to the detail of the wetting ridge are small for a thin lubricating layer so that there is no net energy difference between its final and initial positions. The net surface free energy change is therefore due to the replacement of the oil−vapor interfacial area, ΔA, by an oil−water interface and the increase in the water−vapor or water−oil and oil−

DOI: 10.1021/acs.langmuir.8b04136
Langmuir 2019, 35, 4197−4204

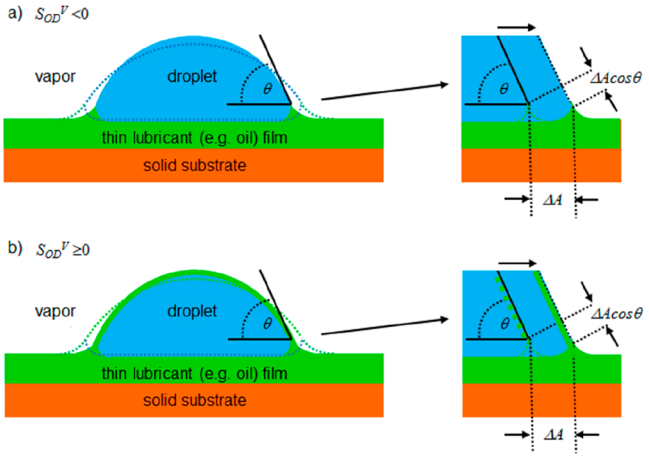

Figure 4. Surface free energy changes due to the small advance, ΔA, of the droplet edge on a smooth SLIP surface (a) without lubricant wrapping ($S_{OD}^{V} < 0$) and (b) with lubricant wrapping ($S_{OD}^{V} \geq 0$). Small-scale texture within which the lubricant is impregnated is omitted for clarity.

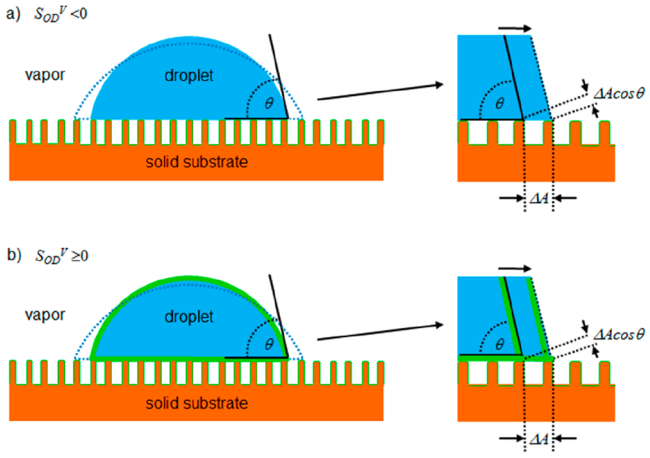

Figure 5. Surface free energy changes due to a one-period advance, $\Delta A(x)$, of the droplet edge on a macrotextured surface possessing a thin conformal SLIPS coating. Cassie–Baxter state (a) without lubricant wrapping ($S_{OD}^{V} < 0$) and (b) with lubricant wrapping ($S_{OD}^{V} \geq 0$). In the latter case, the droplet surface is entirely coated in a thin lubricant layer, including on its underneath surface.

vapor interfacial areas, $\cos\theta\,\Delta A$, depending on whether $S_{OD}^{V} < 0$ or $S_{OD}^{V} \geq 0$. This latter dependence on the spreading power implies that the $\cos\theta\,\Delta A$ change in interfacial area is scaled by either γ_{DV} or by $(\gamma_{DO} + \gamma_{OV})$ (i.e., by γ_{eff}). The first-order change in the surface free energy, ΔF, is therefore

$$\Delta F = (\gamma_{OD} - \gamma_{OV})\Delta A + \gamma_{eff}\Delta A \cos\theta \tag{5}$$

Since this change vanishes when the system is in local equilibrium, $\Delta F = 0$ gives eq 4, which defines the apparent contact angle where θ_{app} is tangent to the profile close to the lubricant surface but is away from any distortion in the droplet profile due to the (small) wetting ridge. Kreder et al.[33] also commented in their work that eq 4 could be obtained by minimizing the energy as well as by balancing forces due to the interfacial tension at the ridge or using a purely geometrical argument. This surface free energy derivation depends on the assumption that at equilibrium a small translational perturbation of the wetting ridge position does not significantly alter the structure of the wetting ridge.

3.2. SLIPS-Modified Cassie–Baxter and Wenzel Equations. The creation of a SLIP surface is achieved using lubricant impregnation of the hydrophobic surface roughness or texture, but this can be part of a multilevel hierarchy of roughness or texture.[17,18,27] For example, a microscale or nanoscale SLIP surface could be part of a macroscale roughness or texture which remains on a length scale much shorter than the capillary length, κ^{-1}, of a droplet. In this case, the SLIP surface becomes a conformal low-pinning lubricant surface of the larger-scale rough or textured macrostructure provided the lubricant does not fill the macrotexture.

Figure 5 shows a small displacement of a droplet edge by one period of pillar-type structure with the same assumptions on the wetting ridge as in section 3.1. The use of a one-period perturbation is an averaging assumption around a droplet perimeter that should be valid when the droplet size is much large than the macrotexture.[37] This perturbation, $\Delta A(x)$, is based on a starting position, x, for the perimeter and so samples whether that position is a local minimum of the surface free energy landscape. Consequently, various parameters are local averages in the vicinity of the perimeter at position x and are not global averages taken across the droplet footprint. If global averages are used for the Cassie solid surface fraction or the Wenzel roughness when the surface has local variations and the Cassie–Baxter and Wenzel equations are applied, inaccurate estimates of the contact angle will occur.[37,38] However, provided parameters local to the perimeter are used, consistent with the surface energy minimization to determine the local equilibrium, the methodology will be valid. This approach is then able to deal with contact angles on surfaces with gradients in topography; for a further discussion, see refs 39 and 40.

The surface free energy changes are composed of three parts: (i) the advance over the tops of microposts, which causes an energy change $(\gamma_{OD} - \gamma_{OV})\varphi_S(x)\,\Delta A(x)$, where $\varphi_S(x)$ is the macrotexture Cassie solid surface fraction local to the droplet perimeter, (ii) the advance over the spaces between microposts, which causes an energy change $\gamma_{eff}(1 - \varphi_S(x))\Delta A(x)$, where γ_{eff} is due to the water from the droplet bridging the space between microposts, which may or may not be covered in a film oil depending on the spreading power (Figure 5a,b), and (iii) the extended droplet surface, which has an additional surface energy of $\gamma_{eff}\cos\theta(x)\,\Delta A(x)$. The total surface free energy change is

$$\Delta F(x) = (\gamma_{OD} - \gamma_{OV})\varphi_S(x)\,\Delta A(x) + \gamma_{eff}(1 - \varphi_S(x))\,\Delta A(x) + \gamma_{eff}\Delta A(x)\cos\theta(x) \tag{6}$$

and setting this change equal to zero gives

$$\cos\theta_{app}^{CB}(x) = \varphi_S(x)\cos\theta_{app} - (1 - \varphi_S(x)) \tag{7}$$

where θ_{app} is defined by eq 4. This is the analogue of the usual simplified form of the Cassie–Baxter equation in which the contact angle has been replaced by the interfacial-tension-defined apparent contact angle, taking into account whether the spreading power of the lubricant on the droplet is positive (or zero) or negative via the effective droplet–vapor interfacial tension, γ_{eff}.

Equation 7 can be applied to the data from Dong et al., who created a doubly re-entrant micropillar-based superoleophobic surface with nanorough pillar tops infused with Krytox-103.[18] These surfaces were tested with droplets of water, ethanol, and

DOI: 10.1021/acs.langmuir.8b04136
Langmuir 2019, 35, 4197–4204

n-octane, giving apparent advancing and receding contact angles of θ_A/θ_R = 160.7°/148.6°, 160.0°/134.3°, and 160.5°/133.0°, respectively, which are similar to the values measured on the non-lubricant-infused structures. We note that Krytox has positive spreading power on water but not on ethanol, so these liquids should include both oil-wrapped and nonwrapped droplets. Their Supporting Information gives apparent advancing and receding angles on a flat nonstructured Krytox-103-infused surface of θ_A/θ_R = 109.9°/107.4°, 56.0°/54.7°, and 47.2°/46.1°. Because they estimated a Cassie fraction φ_S for the macrotexture of between 5 and 8%, eq 4 predicts θ_{app}^{CB} = 161−165, 151−157, and 150−156°, respectively, using the average of the apparent advancing and receding angles on the nonstructured infused surface (i.e., θ_{ave} = 108.7, 55.4, and 46.7°); we believe the use of this average is justified by the low hysteresis on the nonstructured infused surface. The energy minimization approach provides only equilibrium results. On non-SLIPS Cassie−Baxter surfaces, experiments show that droplets adopt contact angles between the advancing and receding contact angles and typically closer to the advancing angle; the range of hysteresis can be large or small depending on the specific surface. The Cassie−Baxter approach therefore predicts an apparent angle between these two. The SLIPS Cassie−Baxter equation gives predictions here that are slightly (∼0−4°) above the measured advancing apparent angle for water and below the apparent advancing but above the apparent receding angle for ethanol and *n*-octane. In the latter two cases, the predicted apparent angles are closer to the measured apparent advancing angles (within ∼3−9 and ∼5−11°, respectively). Thus, eq 7 gives values broadly consistent with the measured advancing apparent contact angles based on the measured average apparent contact angle on the flat nonstructured Krytox-103-infused surfaces. It also illustrates the (usual) insensitivity of the dependence on the precise value of those values, providing a Cassie−Baxter state is achieved. The continued existence of hysteresis in the apparent advancing and receding contact angles on this superoleophobic surface reflects the discrete micropillar texture of the surface. The contact line must still move from the top of one micropillar to another to advance or recede.

A similar approach can be used for the Wenzel case (Figure 6) and gives

$$\cos\theta_{app}^{W}(x) = r_W(x)\cos\theta_{app} \tag{8}$$

where the Wenzel roughness, $r_W(x)$, is the macroscale surface area compared to its horizontal projection at the location of the drop edge. Dai et al. reported apparent contact angle measurements of droplets of water, ethylene glycol, hexadecane, and heptane on Krytox-oil-infused low-aspect-ratio micropillar surfaces with a macrotexture Wenzel roughness of up to r_W = 1.52.[17] They noted that the Wenzel equation using the apparent contact angle was in good agreement with measurements in the high-contact-angle range (i.e., 101.6° < θ_{app} < 121.3°) and at moderate roughness (i.e., r_W < 1.6) but started to deviate at the mid-to-low apparent contact angle range (i.e., 50.9° < θ_{app} < 70.5°) for their data. Their Supporting Information has top-view images (Figure S3) for heptane droplets that show faceted droplets when the roughness is greater than unity. No comments were provided on the faceting of droplets, so it is unclear whether this also applied to droplets of other liquids. This limits the extent to which our model, which assumes axisymmetry, can be applied to the data. It also limits the confidence in reported contact angles, which may depend on the viewing direction.

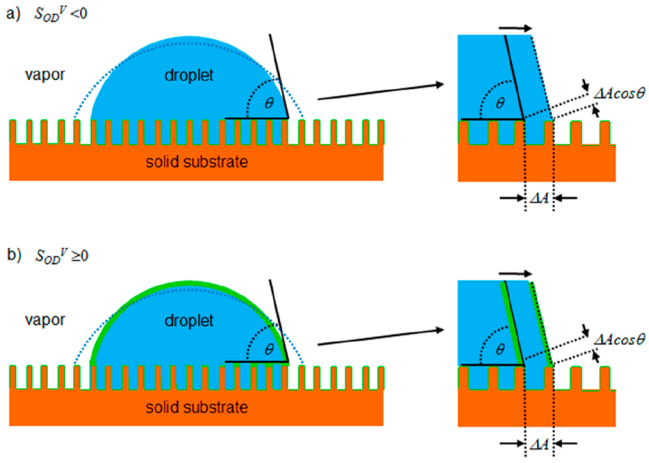

Figure 6. Surface free energy changes due to a one-period advance, $\Delta A(x)$, of the droplet edge on a macrotextured surface possessing a thin conformal SLIPS coating. Wenzel state (a) without lubricant wrapping (S_{OD}^V < 0) and (b) with lubricant wrapping ($S_{OD}^V \geq 0$).

3.3. SLIPS-Modified Hemiwicking and Cassie-to-Wenzel Stability Equations. These ideas can also be applied to other wetting problems involving topography, including hemiwicking and the criteria for the stability of the Cassie−Baxter state and the transition to a Wenzel state.[14] For example, for hemiwicking into a textured surface, the surface free energy change for a liquid (with a liquid labeled D here for consistency with previous sections) to propagate along the texture by one period Δx is $\Delta F(x) = (\gamma_{DO} - \gamma_{OV})(r_W(x) - \varphi_S(x))\Delta A + \gamma_{eff}(1 - \varphi_S(x))\Delta A$ (Figure 7). If this reduces the surface free energy, then liquid will hemiwick into the structure, providing the apparent contact angle, $\theta_{app}(x)$, is smaller than the critical angle, $\theta_c(x)$, defined by

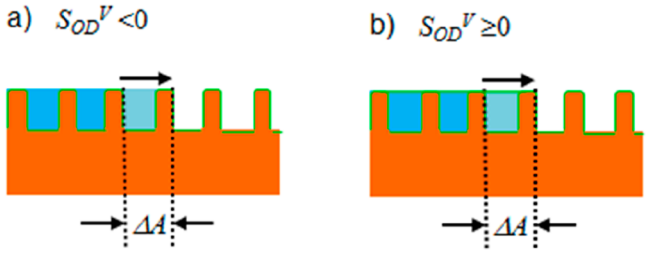

Figure 7. Surface free energy changes for hemiwicking (a) without lubricant wrapping (S_{OD}^V < 0) and (b) with lubricant wrapping ($S_{OD}^V \geq 0$). In the former case, the liquid surface between the pillars does not have a lubricant coating, whereas in the latter case the liquid surface is entirely coated in a thin layer of the lubricant.

$$\cos\theta_c(x) = \frac{1 - \varphi_S(x)}{r_W(x) - \varphi_S(x)} \tag{9}$$

Interestingly, the critical angle defined by eq 9 is the same as for a nonlubricated solid texture and remains at a value determined by its design.

Similarly, the Cassie−Baxter state is energetically preferred over the Wenzel state, provided the apparent contact angle is larger than a critical angle given by $\theta_{st}(x)$, defined by

DOI: 10.1021/acs.langmuir.8b04136
Langmuir 2019, 35, 4197−4204

$$\cos\theta_{st}(x) = -\left(\frac{1-\varphi_S(x)}{r_W(x)-\varphi_S(x)}\right) \tag{10}$$

which gives a critical angle of 180° minus the critical angle for which hemiwicking occurs. Thus, the equations familiar from prior contact angle theory on textured surfaces should apply, provided the contact angle is replaced by the apparent contact angle defined by eq 4.

3.4. SLIPS-Modified Electric-Field-Controlled Apparent Contact Angles. The surface free energy approach taken for understanding apparent contact angles on thin SLIPS-coated topographically structured/textured surfaces can be extended to equilibrium contact angle considerations in other physical systems. In electrowetting on a dielectric, a conducting droplet (typically water with a small concentration of KCl) is used to define one electrical contact on a solid (typically hydrophobic) dielectric surface whose reverse surface is in contact with an electrical conductor.[15,41,42] This forms a capacitive structure, but with the droplet's solid−liquid interfacial contact area forming an electrode with a voltage-dependent area. To determine the equilibrium contact angle changes, the combination of the surface free energy and the capacitive energy changes is minimized, and this leads to a reduction in contact angle with the surface effectively becoming more hydrophilic. A thin SLIPS coating on top of the solid dielectric removes all droplet liquid−solid contacts, but an apparent contact angle still occurs and electrowetting can be performed by applying an external voltage, V.[21] The surface free energy change for a small change in the droplet apparent contact area is given by eq 5, where $\Delta A = 2\pi r\Delta r$ and r is the apparent contact radius. Assuming that any double-layer effects can be ignored, the energy change in charging due to the creation of the additional capacitor area is

$$\Delta U = \frac{-\varepsilon_o\varepsilon_r V^2}{2d} \tag{11}$$

where ε_o is the permittivity of free space, ε_r is the effective relative permittivity of the solid dielectric with the SLIPS coating, and d is total dielectric thickness. Setting the total energy change equal to zero gives the equilibrium condition

$$\cos\theta_{app}(V) = \cos\theta_{app}(0) + \frac{\varepsilon_o\varepsilon_r V^2}{2d\gamma_{eff}} \tag{12}$$

where $\cos\theta_{app}(0)$ is given by eq 4.

An alternative method to controlling a contact angle is to use an applied electric potential of form $V_0e^{-2z/\delta}$, where z is the vertical coordinate normal to the surface and δ is a penetration depth, to create a nonuniform electric field which decays with distance above a substrate and to use a dielectric liquid droplet of relative permittivity ε_l. When the droplet thickness is much larger than δ, changes in the applied voltage V cause the droplet to spread due to the storage of dielectrophoretic energy in the interfacial layer of the dielectric liquid of the droplet.[16,43] Assuming the system is in air, the change in interface-localized liquid dielectrophoretic energy is

$$\Delta U = \frac{-\varepsilon_o(\varepsilon_l - 1)V^2}{2\delta} \tag{13}$$

and the voltage-dependent apparent contact angle for this dielectrowetting becomes

$$\cos\theta_{app}(V) = \cos\theta_{app}(0) + \frac{\varepsilon_o(\varepsilon_l - 1)V^2}{2\delta\gamma_{eff}} \tag{14}$$

In this case, the dielectric properties of the lubricant liquid have been neglected due to the assumption of a sufficiently thin SLIPS coating. Equations 12 and 14 can be written in common notation for electric-field-controlled wetting as

$$\cos\theta_{app}(V) = \cos\theta_{app}(0) + [1-\cos\theta_{app}(0)]\left(\frac{V}{V_{Th}}\right)^2 \tag{15}$$

where V_{Th} is the voltage that would be needed to first create a film (i.e., $\theta_{app}(V_{Th}) \to 0$.[44] These formulas are consistent with the electrowetting and dielectrowetting experimental data presented by Brabcova et al.[21] Their data used a silicone-oil-infused hydrophobic nanoparticle SLIP coating with glycerol as the droplet and demonstrated both significantly reduced hysteresis in the apparent contact angle and linearity of cos $\theta_{app}(V)$ with voltage squared. In this work, a small hysteresis in the apparent contact angle of 3−4° was observed during dielectrowetting but not during electrowetting, which suggests the applied nonuniform electric field caused small changes in the SLIP surface used in the experiment.

4. COMPLEX SURFACE GEOMETRIES AND SHAPES

The ability to predict the apparent contact angle on a thin SLIPS or lubricant-coated surface using eq 4 also allows the equilibrium configuration for a droplet in contact with multiple surfaces or on a complex surface geometry to be predicted.

As an example of the first situation, consider a droplet between and in contact with two planar surfaces which form a wedge of opening angle 2β (inset to Figure 8). For perfectly smooth solid wedges formed by ordinary (non-SLIPS) surfaces, it is well known that when the contact angle of the droplet is between 90° + β and 180° the minimum surface free energy configuration of the droplet is a "liquid-barrel" shape: a spherical segment that intersects the two planes with the

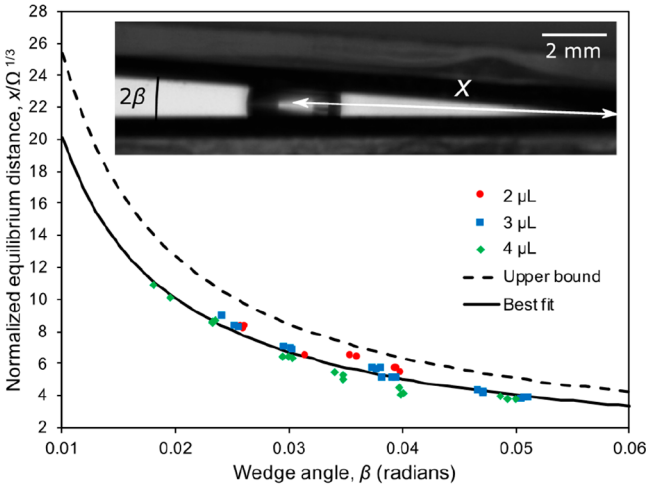

Figure 8. Normalized equilibrium position for a droplet inside a SLIPS wedge. The symbols correspond to experimental measurements; the dashed line corresponds to eq 16 using the upper-bound prediction of eq 4, θ_{app} = 108.4°. The solid line corresponds to a best fit to eq 16 which yields θ_{app} = 103°. Data taken from Ruiz-Gutiérrez et al.[45]

DOI: 10.1021/acs.langmuir.8b04136
Langmuir 2019, 35, 4197−4204

equilibrium contact angle, θ_e.[45,46] The droplet's equilibrium configuration can be described in terms of its radius and its equilibrium distance from the apex of the wedge, both of which are determined by the wedge angle, β, the contact angle, θ_e, and the droplet volume, Ω. This configuration was recently reported by Ruiz-Gutiérrez et al.,[45] who observed liquid-barrel shapes for water droplets, but in their experiment, the implementation used SLIPS wedges (inset to Figure 8). Because eq 4 allows the apparent contact angle to be calculated, the equilibrium position of the droplet in the wedge geometry, x, can now be predicted as a function of the apparent contact angle and the droplet volume using geometry:

$$x(\theta_{app}, \Omega) = -\frac{\cos\theta_{app}}{\sin\beta}\left[\frac{6\Omega}{\pi(\cos(3\theta_{app}) - 9\cos\theta_{app})}\right]^{1/3} \quad (16)$$

In their experiments, Ruiz-Gutiérrez et al.[45] used water droplets on micropatterned SLIP surfaces created via photolithography and infused with silicone oil. Figure 8 shows a comparison of the prediction of eq 16 with the experimental data using the upper-bound apparent contact angle predicted by eq 4, $\theta_{app} = 108.4°$, and a value arising from a best fit of eq 16 to the experimental data, $\theta_{app} = 103°$. This lower value of the apparent angle is reasonable, as the SLIP surfaces in their experiments were infused by dip-coating at relatively low speeds (of about 1 mm s^{-1}) and thus are expected to leave a relatively thick lubricant film similar to the surface shown in Figure 2b.

As an example of the second situation of a complex surface geometry, Wells et al. studied the response of a droplet on a smooth but regularly sinusoidal corrugated SLIP surface.[47] The surfaces were created using a 3D-printer resin and subsequently treated using the nanocoating method reported in Figure 2. On such surfaces, a droplet sits in equilibrium, adopting a shape that intersects the local tangent to the solid with an apparent contact angle $\theta_{app} = 109°$ (cf. Supporting Information in ref 47), which the authors used to successfully predict the stability of the droplet upon evaporation. Remarkably, the experimentally observed apparent angle is almost identical to the angle reported in Figure 2 for SLIPS on a glass substrate ($\theta_{app} = 108.4°$), which further supports the prediction of eq 4 that the apparent contact angle on SLIPS is independent of the underlying solid surface.

5. CONCLUSIONS

In this work, we have considered theoretically how apparent contact angles can be predicted in the thin-layer limit of liquid-infused or lubricant-impregnated surfaces defined by a small wetting ridge. We have argued that equilibrium can be defined for a wide variety of situations by using small surface free energy changes dominated by changes in the lubricant–droplet, lubricant–vapor, and droplet–vapor interfacial areas and that changes in the wetting ridges cause higher-order corrections. On a smooth nontextured surface, this results in an equation analogous to Young's law involving the lubricant–droplet and lubricant–vapor interfacial tensions and an effective interfacial tension for the droplet–lubricant–vapor or droplet–vapor interface depending on whether the oil has a positive spreading power on the droplet. We have shown how this view can justify the use of Cassie–Baxter, Wenzel, hemiwicking, and other topographic contact angle equations using the apparent contact angle based on macroscopic textures that retain a conformal thin SLIP surface coating. We have also argued that the same approach can be applied more widely to contact angle situations, such as electrowetting and dielectrowetting, and to complex surface shapes. Our work provides a conceptual framework which enables results from equilibrium contact angle theory to be applied to a wide variety of surfaces possessing thin lubricant layers for which there is no direct droplet contact with the underlying solid.

AUTHOR INFORMATION

Corresponding Author

*E-mail: glen.mchale@northumbria.ac.uk.

ORCID

Glen McHale: 0000-0002-8519-7986

Rodrigo Ledesma-Aguilar: 0000-0001-8714-0556

Notes

The authors declare no competing financial interest.

ACKNOWLEDGMENTS

G.G.W. acknowledges the financial support of the UK Engineering & Physical Sciences Research Council (EP/P026613/1).

REFERENCES

(1) Young, T. An Essay on the Cohesion of Fluids. *Philos. Trans. R. Soc. London* **1805**, *95*, 65–87.

(2) de Gennes, P. G. Statics and Dynamics: Wetting. *Rev. Mod. Phys.* **1985**, *57* (3), 827–863.

(3) Shirtcliffe, N. J. N. J.; McHale, G.; Atherton, S.; Newton, M. I. M. I. An Introduction to Superhydrophobicity. *Adv. Colloid Interface Sci.* **2010**, *161* (1–2), 124–138.

(4) Bonn, D.; Eggers, J.; Meunier, J.; Rolley, E. Wetting and Spreading. *Surfaces, Interfaces, and Colloids*; John Wiley & Sons, Inc.: New York; pp 415–447.

(5) Deegan, R. D.; Bakajin, O.; Dupont, T. F.; Huber, G.; Nagel, S. R.; Witten, T. A. Capillary Flow as the Cause of Ring Stains from Dried Liquid Drops. *Nature* **1997**, *389* (6653), 827–829.

(6) Erbil, H. Y. Y. Evaporation of Pure Liquid Sessile and Spherical Suspended Drops: A Review. *Adv. Colloid Interface Sci.* **2012**, *170* (1–2), 67–86.

(7) Wong, T.-S.; Kang, S. H.; Tang, S. K. Y.; Smythe, E. J.; Hatton, B. D.; Grinthal, A.; Aizenberg, J. Bioinspired Self-Repairing Slippery Surfaces with Pressure-Stable Omniphobicity. *Nature* **2011**, *477* (7365), 443–447.

(8) Smith, J. D.; Dhiman, R.; Anand, S.; Reza-Garduno, E.; Cohen, R. E.; McKinley, G. H.; Varanasi, K. K. Droplet Mobility on Lubricant-Impregnated Surfaces. *Soft Matter* **2013**, *9* (6), 1772–1780.

(9) Lafuma, A.; Quéré, D. Slippery Pre-Suffused Surfaces. *EPL (Europhysics Lett.* **2011**, *96* (5), 56001.

(10) Guan, J. H.; Wells, G. G.; Xu, B.; Bin; McHale, G.; Wood, D.; Martin, J.; Stuart-Cole, S. Evaporation of Sessile Droplets on Slippery Liquid-Infused Porous Surfaces (SLIPS). *Langmuir* **2015**, *31* (43), 11781–11789.

(11) Harkins, W. D.; Feldman, A. Films. The Spreading of Liquids and the Spreading Coefficient. *J. Am. Chem. Soc.* **1922**, *44* (12), 2665–2685.

(12) Bico, J.; Reyssat, É.; Roman, B. Elastocapillarity: When Surface Tension Deforms Elastic Solids. *Annu. Rev. Fluid Mech.* **2018**, *50* (1), 629–659.

(13) Style, R. W.; Dufresne, E. R. Static Wetting on Deformable Substrates, from Liquids to Soft Solids. *Soft Matter* **2012**, *8* (27), 7177.

(14) Quéré, D. Wetting and Roughness. *Annu. Rev. Mater. Res.* **2008**, *38* (1), 71–99.

DOI: 10.1021/acs.langmuir.8b04136
Langmuir 2019, 35, 4197–4204

(15) Mugele, F.; Baret, J.-C. Electrowetting: From Basics to Applications. *J. Phys.: Condens. Matter* **2005**, *17* (28), R705−R774.
(16) Edwards, A. M. J.; Brown, C. V.; Newton, M. I.; McHale, G. Dielectrowetting: The Past, Present and Future. *Curr. Opin. Colloid Interface Sci.* **2018**, *36*, 28−36.
(17) Dai, X.; Stogin, B. B.; Yang, S.; Wong, T.-S. Slippery Wenzel State. *ACS Nano* **2015**, *9* (9), 9260−9267.
(18) Dong, Z.; Schumann, M. F.; Hokkanen, M. J.; Chang, B.; Welle, A.; Zhou, Q.; Ras, R. H. A.; Xu, Z.; Wegener, M.; Levkin, P. A. Superoleophobic Slippery Lubricant-Infused Surfaces: Combining Two Extremes in the Same Surface. *Adv. Mater.* **2018**, *30* (45), 1803890.
(19) Hao, C.; Liu, Y.; Chen, X.; He, Y.; Li, Q.; Li, K. Y.; Wang, Z. Electrowetting on Liquid-Infused Film (EWOLF): Complete Reversibility and Controlled Droplet Oscillation Suppression for Fast Optical Imaging. *Sci. Rep.* **2015**, *4* (1), 6846.
(20) Bormashenko, E.; Pogreb, R.; Bormashenko, Y.; Aharoni, H.; Shulzinger, E.; Grinev, R.; Rozenman, D.; Rozenman, Z. Progress in Low Voltage Reversible Electrowetting with Lubricated Polymer Honeycomb Substrates. *RSC Adv.* **2015**, *5* (41), 32491−32496.
(21) Brabcova, Z.; McHale, G.; Wells, G. G.; Brown, C. V.; Newton, M. I. Electric Field Induced Reversible Spreading of Droplets into Films on Lubricant Impregnated Surfaces. *Appl. Phys. Lett.* **2017**, *110* (12), 121603.
(22) He, X.; Qiang, W.; Du, C.; Shao, Q.; Zhang, X.; Deng, Y. Modification of Lubricant Infused Porous Surface for Low-Voltage Reversible Electrowetting. *J. Mater. Chem. A* **2017**, *5* (36), 19159−19167.
(23) Abe, J.; Tenjimbayashi, M.; Shiratori, S. Electrospun Nanofiber SLIPS Exhibiting High Total Transparency and Scattering. *RSC Adv.* **2016**, *6* (44), 38018−38023.
(24) Bazyar, H.; Lv, P.; Wood, J. A.; Porada, S.; Lohse, D.; Lammertink, R. G. H. Liquid-Liquid Displacement in Slippery Liquid-Infused Membranes (SLIMs). *Soft Matter* **2018**, *14* (10), 1780−1788.
(25) Luo, J. T. T.; Geraldi, N. R. R.; Guan, J. H.; McHale, G.; Wells, G. G.; Fu, Y. Q. Q. Slippery Liquid-Infused Porous Surfaces and Droplet Transportation by Surface Acoustic Waves. *Phys. Rev. Appl.* **2017**, *7* (1), 014017.
(26) Hui Guan, J.; Ruiz-Gutiérrez, É.; Xu, B.; Bin; Wood, D.; McHale, G.; Ledesma-Aguilar, R.; George Wells, G. Drop Transport and Positioning on Lubricant-Impregnated Surfaces. *Soft Matter* **2017**, *13* (18), 3404−3410.
(27) Kim, P.; Kreder, M. J.; Alvarenga, J.; Aizenberg, J. Hierarchical or Not? Effect of the Length Scale and Hierarchy of the Surface Roughness on Omniphobicity of Lubricant-Infused Substrates. *Nano Lett.* **2013**, *13* (4), 1793−1799.
(28) Zhang, P.; Chen, H.; Zhang, L.; Zhang, D. Anti-Adhesion Effects of Liquid-Infused Textured Surfaces on High-Temperature Stainless Steel for Soft Tissue. *Appl. Surf. Sci.* **2016**, *385*, 249−256.
(29) Kim, P.; Wong, T. S.; Alvarenga, J.; Kreder, M. J.; Adorno-Martinez, W. E.; Aizenberg, J. Liquid-Infused Nanostructured Surfaces with Extreme Anti-Ice and Anti-Frost Performance. *ACS Nano* **2012**, *6* (8), 6569−6577.
(30) Li, Y.; John, J.; Kolewe, K. W.; Schiffman, J. D.; Carter, K. R. Scaling Up Nature: Large Area Flexible Biomimetic Surfaces. *ACS Appl. Mater. Interfaces* **2015**, *7* (42), 23439−23444.
(31) Seiwert, J.; Clanet, C.; Quéré, D. Coating of a Textured Solid. *J. Fluid Mech.* **2011**, *669*, 55−63.
(32) Semprebon, C.; McHale, G.; Kusumaatmaja, H. Apparent Contact Angle and Contact Angle Hysteresis on Liquid Infused Surfaces. *Soft Matter* **2017**, *13* (1), 101−110.
(33) Kreder, M. J.; Daniel, D.; Tetreault, A.; Cao, Z.; Lemaire, B.; Timonen, J. V. I.; Aizenberg, J. Film Dynamics and Lubricant Depletion by Droplets Moving on Lubricated Surfaces. *Phys. Rev. X* **2018**, *8* (3), 31053.
(34) Banpurkar, A. G.; Nichols, K. P.; Mugele, F. Electrowetting-Based Microdrop Tensiometer. *Langmuir* **2008**, *24* (19), 10549−10551.
(35) Peters, F.; Arabali, D. Interfacial Tension between Oil and Water Measured with a Modified Contour Method. *Colloids Surf., A* **2013**, *426*, 1−5.
(36) Rykaczewski, K.; Paxson, A. T.; Staymates, M.; Walker, M. L.; Sun, X.; Anand, S.; Srinivasan, S.; McKinley, G. H.; Chinn, J.; Scott, J. H. J.; et al. Dropwise Condensation of Low Surface Tension Fluids on Omniphobic Surfaces. *Sci. Rep.* **2015**, *4*, 4158.
(37) McHale, G. Cassie and Wenzel: Were They Really so Wrong? *Langmuir* **2007**, *23* (15), 8200−8205.
(38) Gao, L.; McCarthy, T. J. How Wenzel and Cassie Were Wrong. *Langmuir* **2007**, *23* (7), 3762−3765.
(39) Newton, M. I.; Elliott, S. J.; Shirtcliffe, N. J.; McHale, G. Superhydrophobicity: Localized Parameters and Gradient Surfaces. *Contact Angle, Wettability and Adhesion*; Brill Academic Publishers, 2009; Vol. 6, pp 217−234.
(40) McHale, G.; Newton, M. I. M. I.; Shirtcliffe, N. J. N. J. Dynamic Wetting and Spreading and the Role of Topography. *J. Phys.: Condens. Matter* **2009**, *21* (46), 464122.
(41) Berge, B. Electrocapillarity and Wetting of Insulator Films by Water. *C. R. Acad. Des Sci. Ser. II* **1993**, *317* (2), 157−163.
(42) Vallet, M.; Berge, B.; Vovelle, L. Electrowetting of Water and Aqueous Solutions on Poly(Ethylene Terephthalate) Insulating Films. *Polymer* **1996**, *37* (12), 2465−2470.
(43) McHale, G.; Brown, C. V.; Newton, M. I.; Wells, G. G.; Sampara, N. Dielectrowetting Driven Spreading of Droplets. *Phys. Rev. Lett.* **2011**, *107* (18), 186101.
(44) McHale, G.; Brown, C. V.; Sampara, N. Voltage-Induced Spreading and Superspreading of Liquids. *Nat. Commun.* **2013**, *4*, 1605.
(45) Ruiz-Gutiérrez, É.; Guan, J. H.; Xu, B.; McHale, G.; Wells, G. G.; Ledesma-Aguilar, R. Energy Invariance in Capillary Systems. *Phys. Rev. Lett.* **2017**, *118* (21), 218003.
(46) Ruiz-Gutiérrez, É.; Semprebon, C.; McHale, G.; Ledesma-Aguilar, R. Statics and Dynamics of Liquid Barrels in Wedge Geometries. *J. Fluid Mech.* **2018**, *842*, 26−57.
(47) Wells, G. G.; Ruiz-Gutiérrez, É.; Le Lirzin, Y.; Nourry, A.; Orme, B. V.; Pradas, M.; Ledesma-Aguilar, R. Snap Evaporation of Droplets on Smooth Topographies. *Nat. Commun.* **2018**, *9* (1), 1380.

DOI: 10.1021/acs.langmuir.8b04136
Langmuir 2019, 35, 4197−4204